Sequential mechanism of assembly of multidrug efflux pump AcrAB-TolC

Elena B. Tikhonova, **Yoichi Yamada**, and **Helen I. Zgurskaya**[*]
Department of Chemistry and Biochemistry, University of Oklahoma, Stephenson Life Science Research Center, Norman, OK 73019

SUMMARY

Multidrug efflux pumps adversely affect both the clinical effectiveness of existing antibiotics and the discovery process to find new ones. In this study, we reconstituted and characterized by surface plasmon resonance the assembly of AcrAB-TolC, the archetypal multidrug efflux pump from *Escherichia coli*. We report that the periplasmic AcrA and the outer membrane channel TolC assemble high-affinity complexes with AcrB transporter independently from each other. Antibiotic novobiocin and MC-207,110 inhibitor bind to the immobilized AcrB but do not affect interactions between components of the complex. In contrast, DARPin inhibits interactions between AcrA and AcrB. Mutational opening of TolC channel decreases stability of interactions and promotes disassembly of the complex. The conformation of the membrane proximal domain of AcrA is critical for the formation of AcrAB-TolC and could be targeted for the development of new inhibitors.

INTRODUCTION

Antimicrobial drug resistance is the leading challenge in the management of infectious diseases (Levy and Marshall, 2004; Talbot et al., 2006). Some pathogens have acquired resistance to multiple antibiotics and cause infections that are effectively untreatable. Among Gram-negative pathogens, species have emerged which are resistant to all good antibiotics (i.e. with low side effects) and many *Enterobacteriaceae* are resistant to all except carbapenems (Livermore, 2004). Thus, there is a strong need for new approaches to combat multidrug resistant Gram-negative bacteria.

The high intrinsic, as well as acquired antibiotic resistance of Gram-negative pathogens is believed to be a synergistic effect of the active efflux of antibiotics from cells and their slow influx from medium across the outer membrane (Zgurskaya and Nikaido, 2000). The synergy between these two counter directed fluxes is enabled by multidrug efflux pumps, such as AcrAB-TolC from *E. coli*, which actively transport antibiotics from the periplasm or cytoplasm directly into the external medium. The homologs of AcrAB-TolC were identified in all Gram-negative pathogens and implicated in high levels of antibiotic resistance in various clinical isolates (Piddock, 2006).

[*]Corresponding author: Helen I. Zgurskaya, Department of Chemistry and Biochemistry, University of Oklahoma, 101 Stephenson Parkway, Norman, OK 73019. Phone: (405) 325-1678. Fax: (405) 325-6111. elenaz@ou.edu.

The assembly of AcrAB-TolC complex is a mechanistic as well as a methodological conundrum, because two components of the complex, the drug transporter AcrB and the outer membrane channel TolC, are located in two different membranes separated by a periplasm. Previous modeling and genetic studies suggested that AcrAB-TolC complex is assembled into a large protein conduit that spans both membranes of *E. coli* and the periplasm (Bavro et al., 2008; Fernandez-Recio et al., 2004; Husain et al., 2004; Mikolosko et al., 2006; Murakami et al., 2002; Seeger et al., 2006; Symmons et al., 2009). In this complex, the inner membrane transporter AcrB and the outer membrane channel TolC form stable trimers extending deep into the periplasm. The large periplasmic domains of AcrB and TolC meet halfway across the periplasm and match each other in the size and geometry suggesting that these two proteins could interact with each other. A direct interaction between AcrB and TolC was supported by *in vivo* cysteine cross-linking studies and genetic experiments (Tamura et al., 2005; Weeks et al., 2010).

The proposed interface between AcrB and TolC appears to be limited to the apices of their periplasmic domains (Bavro et al., 2008; Symmons et al., 2009). This observation prompted an idea that AcrB-TolC complex is stabilized by the periplasmic membrane fusion protein (MFP) AcrA. In crystals, AcrA has an elongated modular structure that enables interactions with both AcrB and TolC located in the inner and outer membranes, respectively (Mikolosko et al., 2006). The cross-linking and computer modeling studies suggested that three domains of AcrA, namely lipoyl-binding, α–β-barrel and membrane proximal (MP), interact with the periplasmic domain of AcrB, whereas its α-helical hairpin binds TolC (Lobedanz et al., 2007; Symmons et al., 2009). The bi-partite AcrA-AcrB and AcrA-TolC interactions have been demonstrated *in vitro* (Tikhonova et al., 2009; Tikhonova and Zgurskaya, 2004; Touze et al., 2004). However, the reconstitution of the complete tri-partite complex has not been achieved.

Since in *E. coli* the outer membrane component of the complex is shared by multiple transporters, current models postulate that TolC is engaged by a particular inner membrane transporter only transiently (Zgurskaya, 2009). The periplasmic MFPs, such as AcrA, are proposed to play an important role in this process by trapping TolC into a complex. In agreement, MFPs that function with various efflux pumps were found to differ in their affinities toward TolC suggesting that the recruitment of TolC into efflux complexes is under kinetic control (Tikhonova et al., 2009). It remains unclear at what step during the complex assembly TolC binds AcrB and whether or not this interaction affects AcrA-TolC interactions. Furthermore, in the assembled complex, TolC is believed to adopt an open conformation that promotes diffusion of drugs through the TolC channel into the medium. Whether binding of AcrA, AcrB or both components trigger this conformation transition in TolC is under debate.

In this study, we used a surface plasmon resonance approach to investigate interactions between components of AcrAB-TolC complex and a possible role of substrates and inhibitors in the assembly of the complex. We report the reconstitution and analysis of all interactions within the AcrAB-TolC complex.

RESULTS

Immobilization of AcrB

To immobilize AcrB on a surface in a specific orientation, we constructed AcrB containing a single cysteine residue on its C-terminus. For this purpose, the two native cysteine residues C493 and C887 of AcrB were replaced with serines (AcrB^{CL}) and a single S1043C substitution was introduced by site-directed mutagenesis (AcrB^{S1043C}). When produced from plasmids along with AcrA, both AcrB^{CL} and AcrB^{S1043C} complemented the drug

susceptible phenotype of *ΔacrAB* cells demonstrating that mutations did not disrupt multidrug efflux activity (Table 1S).

A biotin moiety was attached to the C1043 of purified AcrB[S1043C] (Cys1043[bio]) using a thiol-reactive reagent biotin-maleimide (Figure 1A). The light scattering coupled to size exclusion HPLC (LS-SEC) showed that Cys1043[bio] is eluted from the column as a major peak (B14) preceded by a shoulder (B11) (Figure 1B). Based on the light scattering measurements these peaks correspond to AcrB dimers and trimers with molecular masses 244 ± 7 and 379 ± 11 kDa, respectively. A minor peak eluted the last from the column is likely composed of AcrB monomers. This result is consistent with previous reports (Stroebel et al., 2007) that gel filtration separates AcrB into a heterogeneous mixture of quaternary structures. The chemical cross-linking however showed that the predominant oligomeric form of Cys1043[bio] is a trimer (Fig. 1C). Thus, separation on the column promotes dissociation of AcrB trimers.

A streptavidin coated SA chip was used to capture Cys1043[bio] and its B11 and B14 fractions onto surface (AcrB thereafter). To assess the binding capacity and the conformational state of immobilized AcrB, we used inhibitor DARPin, which binds the periplasmic domain of AcrB trimer with 2:3 stoichiometry and has a strong preference to the Tight (T) and Loose (L) protomers of AcrB (Sennhauser et al., 2007). In agreement with previous studies we found that DARPin binds AcrB with low nanomolar affinity and follows a simple 1:1 Langmuir kinetics (Figure 1D). The simple kinetics of DARPin binding implies that immobilized AcrB is homogeneous. DARPin bound the B14 and B11 fractions of AcrB with comparable efficiencies suggesting that both these fractions are immobilized in a structurally competent trimeric form (Figure 1E). At saturation, the calculated stoichiometry of DARPin:AcrB was close to 2:3, which is consistent with the earlier findings that two DARPin molecules bound per one asymmetric AcrB trimer (Sennhauser et al., 2007).

Immobilized AcrB binds substrates and inhibitors

We tested several antibiotics, the known substrates of AcrB, for their ability to bind the immobilized transporter. At pH 7.5, antibiotic novobiocin and the broad spectrum efflux pump inhibitor MC-207,110 (Lomovskaya et al., 2001) produced strong binding responses (Figure 2A and 2D). These analytes however, bound AcrB surface with on and off rates, which are too fast for kinetic modeling. Analysis of the association equilibrium data showed that binding of MC-207,110 and novobiocin to AcrB could be reasonably well approximated by 1:1 binding kinetics with dissociation equilibrium constants (K_D) in the high micromolar range (Figure 2B and 2E). Decreasing pH to 6.0 increased affinity of MC-207,110 toward AcrB (Figure 2B). Novobiocin precipitated from solution at pH 6.0 and its binding to AcrB could not be studied at this pH.

We also tested other water soluble substrates of AcrB including antibiotics oleandomycin, ampicillin and cloxacillin. No specific binding response was detected for these molecules (data not shown). Perhaps the low affinity and small size of these analytes precludes analysis of their binding to AcrB by SPR.

Lipidation of AcrA is essential for high affinity binding to AcrB

Previous structural and biochemical analyses of AcrA and AcrAB complex were carried out with the soluble variant of AcrA lacking the N-terminal lipid modification (AcrA[s]) (Figure 3A) (Mikolosko et al., 2006; Touze et al., 2004; Zgurskaya and Nikaido, 1999b). When AcrA[s] was injected over AcrB surface the binding response was very low both at pH 7.5 and pH 6.0 (Figure 3B). The injection of the native lipid-modified AcrA (AcrA[l]) however, resulted in a strong binding response at pH 6.0 but not at pH 7.5.

Analysis of the two AcrA variants by LS-SEC showed that lipid modification of AcrA promotes oligomerization. Consistent with previous reports AcrA[s] was eluted from the column as a single symmetric peak with molecular weight ~40 kDa at both pH 7.5 and 6.0 (Figure 3C). In contrast, the elution profile of AcrA[l] was heterogeneous and depended on pH of the buffer (Figure 3D). At pH 6.0, the molecular mass of AcrA[l] in the major peak was found to be 100±4 kDa, which corresponds to AcrA dimer. The AcrA[l] dimer peak was preceded by a shoulder, which could comprise an AcrA[l] conformer or a trimer. The increase of pH to 7.5 led to a dramatic change of the elution profile with appearance of large amounts of higher-order AcrA[l] oligomers (Figure 3D).

To determine which form of AcrA[l] has higher affinity to AcrB, AcrA[l]-containing fractions eluted from the gel filtration column at pH 6.0 were injected over immobilized AcrB and its B11 and B14 fractions. On all three surfaces, the strong binding response was obtained only for fractions containing dimeric AcrA[l] (Figure 3E). Thus, the lipidation-dependent AcrA[l] dimerization promotes high affinity binding to AcrB.

We next compared the proteolytic patterns of AcrA[l] and AcrA[s] generated by trypsin digest to further investigate the effect of lipidation and oligomerization on AcrA structure (Figure 3F). Although both AcrA variants were cleaved into the same set of fragments, the T47-K346 fragment of AcrA[l] was notably more resistant to cleavage than the corresponding fragment of AcrA[s]. This result suggested that AcrA[l] oligomerization leads to protection of R315 residue located in the MP domain of AcrA[l] (Figure 3A).

Previously, we found that G363C substitution in the MP domain of AcrA[l] (AcrA[G363C]) disrupts the multidrug efflux activity of AcrAB-TolC (Ge et al., 2009). To determine whether the MP domain is indeed important for the AcrA-AcrB interaction, we purified AcrA[G363C] and compared its properties to those of AcrA[l] and AcrA[s]. In agreement with previous studies (Ge et al., 2009), cells producing AcrA[G363C] were significantly more susceptible to multiple antibiotics (Table 1S). The SEC elution profile of AcrA[G363C] matched that of AcrA[l] demonstrating that this substitution does not change the oligomeric state of AcrA[l] (Figure 3D). Accordingly, the SDS-PAGE analysis under non-reducing conditions confirmed that AcrA[G363C] is a dimer covalently linked by a disulfide bond (Figure 3G). The proteolytic pattern of AcrA[G363C] however was distinct from both AcrA[s] and AcrA[l] (Figure 3F). The amounts of T47-K346 fragment of AcrA[G363C] were similar to those in the AcrA[l] pattern. At the same time, the Q29-K374 and T47-K396 fragments, which were rapidly cleaved in both AcrA[s] and AcrA[l], became the major bands in the AcrA[G363C] pattern. This result suggests that the G363C substitution changes the structure of the MP domain. The SPR experiments further showed that the structural changes caused by G363C substitution are unfavorable for AcrA interaction with AcrB. The rate of association of AcrA[G363C] with immobilized AcrB was visibly slower than that of AcrA[l] (Figure 3B).

Taken together, these results demonstrate that the N-terminal lipidation promotes AcrA oligomerization and stabilizes its MP domain. We further conclude that the structure of the MP domain is essential for the interaction between AcrA and AcrB.

AcrA binds AcrB with nanomolar affinity

To analyze kinetics of AcrA-AcrB interactions, increasing concentrations of AcrA[s], AcrA[l] and AcrA[G363C] were injected over AcrB surface at pH 6.0 (Figure 4 and Table 1). For AcrA[s], the data fit well to a simple 1:1 binding model with the equilibrium dissociation constant K_D= 1.2 μM (Figure 4A). In contrast, the quantitative analysis of the AcrA[l] and AcrA[G363C] curves showed complex reactions (Figure 4B and 4C). The association and dissociation phases could be best approximated using double-exponential rate equations, indicating multiple reaction events. The best fit of AcrA[l]-AcrB and AcrA[G363C]-AcrB

binding curves was obtained for the model that assumes conformational change upon association (Two-state reaction, TS). Based on this model, the initial association event (k_1 in Table 1) was characterized by the moderate rates ~10^4 M^{-1} s^{-1} for both AcrA variants. However, association of AcrA^{G363C} with AcrB was 44% slower than that of AcrA^l. Furthermore, G363C substitution led to about two-fold increase in the off-rates for both steps indicating the decreased stability of AcrA-AcrB complex. The K_D= 0.23 μM and K_D= 0.09 μM for AcrA^{G363C} and AcrA^l, respectively, were at least 5–10 fold higher than the K_D of AcrA^s.

To investigate possible effects of substrates and inhibitors on AcrA-AcrB interactions, we mixed AcrA^l and inhibitors in different molar ratios and injected them over the immobilized AcrB. We found no significant effect on AcrA-AcrB interactions by antibiotics oleandomycin and novobiocin and inhibitor MC-207,110 at up to 100 molar excess of drug over AcrA (Figure 4D). In contrast, increasing concentrations of DARPin significantly inhibited binding of AcrA^l to AcrB (Figure 4E). Even at submolar DARPin:AcrA^l ratios, the AcrA^l binding response decreased up to 80%. Since no interaction between DARPin and AcrA^l was detected (data not shown), we conclude that binding of DARPin to AcrB interferes with the assembly of AcrA^l-AcrB complex.

TolC binds AcrB independently from AcrA

Structural and genetic studies suggested that TolC could directly interact with AcrB but the extent and timing of such interaction is unclear (Bavro et al., 2008; Tamura et al., 2005). To investigate AcrB-TolC interaction, the increasing concentrations of purified TolC were injected over AcrB surfaces at pH 6.0 and 7.5 (Figure 5A and 5B). At both pHs, TolC interacted specifically with AcrB but at the same concentrations TolC binding signal at pH 6.0 was more than ten times higher than at pH 7.5. TolC interacted with AcrB surface, which was never exposed to AcrA excluding the possibility that traces of AcrA on the AcrB surface are responsible for the observed TolC-AcrB interaction. Binding of TolC to AcrB was insensitive to the presence of oleandomycin but decreased by 30–40% in the presence of novobiocin and MC-207,110 (Figure 5C).

The best fit of AcrB-TolC curves was also obtained for the TS model (Figure 5B). Based on this model, the initial association with AcrB was significantly faster for TolC than for AcrA^l (Table 1). However, the slower conformational transition steps were similar for the two proteins. The equilibrium dissociation constant for TolC-AcrB complex derived from the rates shown in Table 1, K_D~ 0.09 μM, was similar to that for AcrA^l-AcrB complex. Thus, TolC binds AcrB directly and with the high affinity.

Mutational opening of the TolC channel decreases its affinity toward AcrA and AcrB

Structural and modeling studies suggested that the best fit between TolC and AcrB is achieved when TolC is modeled in its proposed open conformation (Bavro et al., 2008; Symmons et al., 2009). We next constructed TolC mutant containing Y362F and R367E substitutions in its periplasmic domain (TolC^{YFRE}). These mutations destabilize the critical salt bridges in the periplasmic entrance of TolC and trigger partial opening of the channel (Andersen et al., 2002; Bavro et al., 2008). In agreement with previous studies, TolC^{YFRE} protected *E. coli*, albeit only partially, from various antimicrobials indicating that this mutant is assembled into the multidrug efflux complex (Table 1S). TolC^{YFRE} was then purified and compared to the wild type protein in binding to immobilized AcrA and AcrB.

To characterize AcrA-TolC^{YFRE} interactions, we used AcrA^{S362C} mutant with a single cysteine substitution in the position 362, which, in contrast to AcrA^{G363C}, is fully functional in multidrug efflux (Ge et al., 2009). For immobilization, AcrA^{S362C} was modified with

biotin-maleimide and captured onto the SA chip under the same conditions as AcrB. TolC[YFRE] was next injected either over AcrA or AcrB surface and its binding affinity compared to that of the wild type TolC. The mutational opening of TolC[YFRE] significantly affected its interactions with both AcrA and AcrB proteins (Figure 5D and 5E).

In agreement with the previous studies (Tikhonova et al., 2009), the best fit for AcrA-TolC binding was obtained for the model that assumed the presence of two populations of ligand on the surface with fast and slow dissociation rates. Based on this model, the affinities of TolC to two populations of AcrA were $K_{D1} = 0.01$ μM and $K_{D2} = 0.11$ μM for the slow and fast complexes, respectively. The rate and equilibrium constants derived from the kinetic analysis of TolC[YFRE] interaction with AcrA showed the notably lower affinity with $K_{D1} = 0.02$ μM and $K_{D2} = 6.7$ μM for the slow and fast complexes, respectively.

As with TolC, binding of TolC[YFRE] to AcrB fit best to the TS model (Figure 5F). The initial association, k_1, and the second dissociation, k_{-2} rates for TolC[YFRE] were two times slower than the corresponding rates for the wild type protein. However, the equilibrium dissociation constants, $K_D \sim 0.1$ μM, were very similar for TolC-AcrB and TolC[YFRE]-AcrB complexes (Table 1). This result shows that the conformation of the periplasmic tip of TolC affects the rates of binding without changing the equilibrium of the reaction.

Mutations in the periplasmic entrance of TolC[YFRE] move the three pairs of coiled coils radially outward from the central molecular axis (Bavro et al., 2008). The greatest conformational changes occur in the H7/H8 helices and lead to the widening of the entrance and deepening of the proposed AcrA binding grooves. If in solution TolC[YFRE] retains the same conformation, our data suggest that this conformation is unfavorable for both TolC-AcrB and TolC-AcrA interactions and could promote faster dissociation of AcrAB-TolC complex. The decreased affinity of TolC[YFRE] to AcrAB is consistent with the partial activity of TolC[YFRE] in multidrug efflux (Table 1).

Sequential assembly of AcrAB-TolC complex

The described above experiments established that TolC binds both AcrA and AcrB with affinities in the nanomolar range. To study the assembly of the three-component AcrAB-TolC complex, AcrA[1] and TolC were pre-mixed together at different molar ratios and injected over the AcrB surface (Figure 6A). Using this approach we found no evidence for the formation of AcrAB-TolC complex. Furthermore, even at submolar ratios, TolC inhibited assembly of AcrA-AcrB complexes, possibly because TolC binding to AcrA in solution interfered with AcrA-AcrB interactions on the surface (Figure 6A).

We next used a sequential co-injection approach to separate in time the bi-partite interactions leading to the assembly of AcrAB-TolC complex (Figure 6B–E). In these experiments, AcrA-AcrB or TolC-AcrB complexes are assembled during the first injection and then exposed to the respective third component in the second injection. If the tri-partite complex is assembled on the surface, then the second injection is expected to increase the amounts of AcrA or TolC bound to AcrB. As shown on Figure 6B, the pre-assembly of TolC-AcrB complexes on the surface followed by injection of AcrA increased the amounts of bound TolC suggesting that the three-component complex is assembled but its amounts are low (shaded area; Figure 6B). Surprisingly, replacement of AcrA in the above reactions with its AcrA[G363C] variant led to a notable ~20% increase in the amounts of the retained TolC and correspondingly, AcrAB-TolC complexes (shaded area, Figure 6C). Thus, the conformational change induced by G363C substitution in AcrA is favorable for the tri-partite interactions. The assembly of the tri-partite complex was also seen when AcrA-AcrB complex was pre-assembled first followed by the injection of TolC (data not shown). The

inclusion of oleandomycin into binding reactions did not affect the assembly of the complexes.

When TolC was substituted with its open variant TolC[YFRE], we found no evidence of tripartite interactions (Figure 6D and 6E). This result strongly suggests that AcrAB-TolC complex is assembled with the closed conformer of TolC.

Taken together these results provide a strong experimental evidence for the independent assembly of TolC-AcrB and AcrA-AcrB complexes (Figure 6F). However, the pre-assembly of AcrA-TolC in solution interferes with AcrA binding to AcrB indicating a sequential mechanism of the assembly. The complete three-component AcrAB-TolC complex is favored with AcrA[G363C] variant. Since G363C substitution affects the AcrA MP domain, we conclude that the conformation of this domain is important not only for AcrA-AcrB interactions but also for the assembly of AcrAB-TolC.

DISCUSSION

Extensive *in vivo* and *in vitro* studies yielded a model of the three-component AcrAB-TolC complex (Koronakis et al., 2000; Lobedanz et al., 2007; Mikolosko et al., 2006; Seeger et al., 2006). However, how this complex is assembled remains unclear. In this study, we succeeded in reconstitution of the bi-partite AcrA-AcrB and TolC-AcrB and the full AcrAB-TolC complexes and characterized kinetics of these interactions. Our data suggest that AcrA-AcrB and TolC-AcrB complexes are formed independently and that conformation of the MP domain of AcrA is critical for the assembly of the tri-partite complex.

In this study, we addressed three highly debatable questions about the assembly of AcrAB-TolC pump. The first question is about the oligomeric state of AcrA. All MFPs are prone to oligomerization albeit to a different degree and with different affinities (Tikhonova et al., 2009). Several indirect findings indicated that MFPs associated with RND-type pumps, such as AcrA, might bind a transporter in their dimeric forms (Bavro et al., 2008; Fernandez-Recio et al., 2004; Misra and Bavro, 2009; Zgurskaya et al., 2009). However, the chemical cross-linking *in vivo* and structural modeling experiments of AcrAB-TolC suggested that AcrA is a monomer when bound to AcrB (Symmons et al., 2009). Our data provide a strong support for the model, in which a dimeric AcrA binds an AcrB protomer establishing the stoichiometry of AcrA-AcrB complex at 6:3. First, the affinity of AcrA[l] to AcrB is by an order of magnitude higher than that of the soluble variant (Figure 4). Our results show that this increase in affinity is due to stabilization of the MP domain and AcrA[l] oligomerization (Figure 3). Second, AcrA[G363C] is a dimer covalently linked by a disulfide bond (Figure 3G). Yet this mutant bound AcrB with affinity comparable to that of AcrA[l] excluding the possibility that AcrA monomerization is needed for complex formation. Finally, DARPin inhibits binding of AcrA[l] (Figure 4E). In the crystal structure of AcrB-DARPin complex (Sennhauser et al., 2007), DARPin occupies only one of the two putative AcrA binding sites of AcrB. Therefore, the inhibitory effect of DARPin is consistent with two AcrA molecules bound per AcrB protomer. However, alternative explanations such as the inhibitory effect of DARPin on conformation of AcrB cannot be excluded at this point. Taken together these results strongly support the notion that AcrA dimers associate with AcrB (Figure 6F).

The second question is how TolC is assembled into a complex. Although it is broadly believed that AcrA is needed to engage TolC into the complex (Koronakis et al., 2004; Nikaido and Takatsuka, 2009; Pos, 2009; Zgurskaya, 2009), our results strongly suggest that TolC interaction with AcrB is independent from AcrA. The equilibrium dissociation constants for AcrA-AcrB and TolC-AcrB complexes are in the same nanomolar range (Table 1). However, the initial association rate for the TolC-AcrB complex is at least 4 fold

faster than for AcrA-AcrB complex indicating that TolC-AcrB interactions are more dynamic than those in AcrA-AcrB complex. Previously, the TolC-AcrB complex was proposed based on complementary distributions of charges in the periplasmic tips of TolC and AcrB and on *in vivo* disulfide cross-linking of cysteine residues positioned in the putative contacting loops of the two proteins (Bavro et al., 2008; Tamura et al., 2005). Our experiments provide a first biochemical evidence of TolC-AcrB complex and further demonstrate that this complex is formed even in the absence of AcrA. We propose that AcrA and TolC bind AcrB independently and that the tri-partite complex is assembled between AcrA and TolC bound to AcrB (Figure 6F).

Finally, the AcrAB-TolC model guided by *in vivo* cross-linking data could only be assembled by altering the conformations of both AcrA and TolC (Symmons et al., 2009). The proposed structure involves the forced opening of the periplasmic entrance of TolC channel, which leads to the close fit between the apex of the tip of TolC and AcrB and deepening of the intraprotomer groove between the H3/H4 and H7/H8 helices of TolC. This intraprotomer groove is proposed to be a high affinity site for AcrA needed for stabilization of the open conformation of TolC (Bavro et al., 2008). We found however, that the partial opening of TolC by removing the critical salt bridges in the tip of TolC is unfavorable and leads to destabilization of both TolC-AcrB and TolC-AcrA complexes, with the most profound effect on TolC-AcrA (Figure 5). Furthermore, we found no evidence for the tri-partite complex assembled with TolC[YFRE] (Figure 6). This result suggests that instead of stabilization, TolC opening could lead to disassembly of AcrAB-TolC (Figure 6F). However, we cannot exclude a possibility that the conformation of TolC[YFRE] does not approximate the "true" open conformation of TolC and its structural asymmetry is the reason for the lower affinity toward AcrA (Bavro et al., 2008; Pei et al.).

The assembly of the tri-partite AcrAB-TolC complex is most evident with AcrA[G363C] mutant, in which the conformation of the MP domain differs from that of the wild type protein (Figure 6C). The proposed AcrA-AcrB interface is quite extensive and involves the three out of four domains of AcrA: the lipoyl, the β-barrel and the MP (Symmons et al., 2009). The limited proteolysis experiments showed that the major changes in AcrA structure caused by G363C substitution are localized to the MP domain (Figure 3F). Since the AcrA structure is very dynamic and allows significant interdomain flexibility (Ip et al., 2003; Mikolosko et al., 2006), it is possible that the conformation of the MP domain is important for AcrA to engage into a tripartite association with AcrB and TolC. Perhaps *in vivo* or in membranes, binding to AcrB is sufficient to trigger conformational changes in AcrA needed for a complex formation. In detergents however, such conformation was promoted by G363C substitution in the AcrA MP domain. We propose that in AcrA[G363C]-AcrB complex, the orientation of AcrA is such that the α-helical hairpin can reach and bind TolC already engaged into a complex with AcrB (Figure 6F). Importantly, open TolC[YFRE] mutant does not engage AcrA[G363C] (Figure 6E).

The interactions between components of the AcrAB-TolC complex were not stimulated by the presence of substrates and even were slightly inhibited by novobiocin and MC-207,110. Furthermore, among various compounds only binding of novobiocin and MC-207,110 to AcrB could be detected and reproduced consistently. Small molecule binding is often difficult to detect in SPR assays because of the low signal. In contrast, novobiocin and MC-207,110 binding responses on AcrB surface were unexpectedly high suggesting either multiple binding sites or underestimation of their effective masses (Figure 2). It is possible that the large signal of these compounds is caused by formation of homotypic aggregates or mixed detergent-inhibitor micelles. Lastly, the periplasmic concentrations of AcrA and TolC are estimated to be ~100 and ~3 μM, respectively (Tikhonova and Zgurskaya, 2004). These concentrations are well above the nanomolar K_{DS} for interactions between components of

the complex (Table 1) and imply that *in vivo* AcrB exists in the complex with AcrA and TolC. Therefore, inhibitors with high micromolar activities are unlikely to act by inhibiting the interactions between components of AcrAB-TolC complex.

SIGNIFICANCE

We describe the reconstitution of multidrug efflux pump AcrAB-TolC that functions in the context of two membranes of *E. coli*. Our results show that the tri-partite complex is assembled between AcrA and TolC bound to AcrB with high affinities. The likely stoichiometry of AcrA:AcrB:TolC is 6:3:3. Antibiotics and MC-207,110 inhibitor do not modulate interactions between components of the complex. The inhibitory effect of DAPRin on AcrAB-TolC function is due to inhibition of AcrA-AcrB interactions. We report biochemical assays that could be readily adapted for screening of novel inhibitors that interfere with AcrAB-TolC assembly and potentiate diverse antimicrobial agents. The conformational change in the MP domain of AcrA appears to be a "bottleneck" in the assembly of the tri-partite complex and could be targeted for development of effective inhibitors of AcrAB-TolC assembly.

EXPERIMENTAL PROCEDURES

Purification of proteins

Construction and purification of AcrA[l], AcrA[G362C], AcrA[G363C], AcrA[s] and TolC containing the C-terminal six histidine (6His) affinity tags were reported before (Ge et al., 2009; Tikhonova et al., 2009; Zgurskaya and Nikaido, 1999a). AcrA[s] lacking the signal peptide and C25, the site of lipid modification, was overproduced in and purified from the cytoplasm (Zgurskaya and Nikaido, 1999a). The native AcrA[l] was purified from the membrane fraction (Ge et al., 2009). Plasmid producing a cysteine-less AcrB variant and the purified DARPin (MW=18.2 kDa) were a gift from Dr. Olga Lomovskaya. All other mutants were constructed using QuickChange site-directed mutagenesis kit (Stratagene). AcrB[S1043C] without an affinity tag was purified using Cu^{2+} affinity chromatography as described previously (Zgurskaya and Nikaido, 1999b). Protein concentrations were determined using the Protein DC assay (Bio-Rad) and bovine serum albumin as a standard.

Light scattering and size exclusion chromatography (LS/SEC)

Proteins were analyzed by HPLC (Shimadzu) using YMC-Pack Diol-300 size exclusion column. Protein samples (0.4–1.2 mg/ml) were injected in the buffer containing 20 mM MES-KOH (pH 6.0), 0.03% dodecyl maltoside (DDM) and 150 mM NaCl (MES buffer) at the flow rate of 0.5 or 1.0 ml/min. For pH 7.5, MES-KOH was substituted with 20 mM Tris-HCl (Tris buffer). The light scattering (LS) and refraction index (RI) of eluted proteins was measured using PD2010 light scattering detector (Precision Detectors, MA) and Waters 2414 detector, respectively. The molecular mass of the proteins was calculated from the LS and RI data using Discovery software (Precision Detectors, MA) as described earlier (Petrushenko et al., 2006).

Surface Plasmon Resonance

A BIAcore 3000 biosensor system was used to characterize binding interactions. Disulfide bonds of purified AcrB[S1043C] and AcrA[S362C] were reduced using Tris[2-carboxyethyl]phosphine hydrochloride disulfide reducing gel (Pierce) in buffer containing 20 mM Tris-HCl (pH 7.0), 500 mM NaCl, 5 mM EDTA and when needed, 0.03% DDM. Biotinylation of AcrB[S1043C] and AcrA[S362C] was carried out with maleimide-PEG$_2$-Biotin (Pierce) at 1:20 protein:biotin molar ratio in the same buffer for 2 h on ice. Unreacted biotin-maleimide was removed from proteins by gel filtration on a NAP-5 column (GE

HealthCare) followed by overnight dialysis against 20 mM Tris-HCl (pH 7.5), 500 mM NaCl, 0.03% DDM. Biotinylation was confirmed by separating 1.0 µg of a biotinylated protein on 10% SDS-PA gel followed by blotting onto a PVDF membrane. The membrane was then treated with streptavidin-alkaline phosphatase conjugate (Sigma) and a biotinyl-protein conjugate visualized with NBT/BCIP reagents (Bio-Rad).

Biotinylated proteins were immobilized onto SA biosensor chip (Biacore) in Tris buffer. Surface activation and coupling procedures were carried out as recommended by the manufacturer (GE Healthcare). To develop an SPR-based binding assay, Cys1043[bio] was coupled to a SA biosensor chip surface to various densities. A coupling density of 2,000 Response Units (RU) corresponds to 2 ng/mm^2 or ~1000 AcrB molecules/µm^2. This translates into the concentration of immobilized AcrB ~180 µM. For comparison, *E. coli* cells contain approximately 500 copies of AcrB per cell (Tikhonova and Zgurskaya, 2004). If modeled as an ellipsoid with the surface area 2.4 µm^2, an *E. coli* cell contains ~200 AcrB molecules/µm^2 of the inner membrane.

As a control we used an untreated SA surface. All experiments were carried out in MES buffer (pH 6.0) or Tris buffer (pH 7.5). Analytes (proteins, inhibitors and substrates) were diluted in running buffers. Between each analyte injection the surface was regenerated by brief injection of 40 mM CHAPS prepared in 20 mM Tris-HCl (pH 8.0); 150 mM NaCl and 0.03% DDM. For reproducibility purposes all injections were done in repetitions and on different surfaces. To minimize mass transfer effects, the flow rate of injections was kept at 50 µl/min. All shown sensograms are normalized by subtracting responses from the control AcrB-free surface.

Kinetic analysis of TolC-AcrB and AcrA-AcrB interactions

Data were analyzed with BiaEvaluation ver. 6 and Microsoft Excel software. At pH 6.0, both the association and dissociation phases of TolC-AcrB and AcrA-AcrB SPR sensorgrams could be approximated as double exponential decays. Such kinetics rules out simple reaction mechanisms and predicts at least two distinct events during both protein binding and dissociation. The best global fit for both AcrA-AcrB and TolC-AcrB was obtained using the Two-State reaction (TS) model. Schematic representation and equations relevant to this model are given below:

$$A+B \leftrightarrow A \bullet B \leftrightarrow [A \bullet B*] \tag{1}$$

$$\frac{\partial (A \bullet B)}{\partial t} = k_1[A][B] - (k_{-1}[A \bullet B] - k_{-2}[A \bullet B*]) \tag{2}$$

$$\frac{\partial (A \bullet B*)}{\partial t} = k_2[A \bullet B*] - k_{-2}[A \bullet B*] \tag{3}$$

$$R_t = [A \bullet B] + [A \bullet B*] \tag{4}$$

The equilibrium dissociation constant for this model is:

$$K_D = \frac{k_{-1}k_{-2}}{k_1 k_2}$$

(5)

where [A] is the concentration of analyte, [B] is the ligand binding capacity, [A•B] and [A•B*] are intermediate and final complexes, respectively, k_{-1}, k_{-2}, k_1 and k_2 are microscopic rate constants, and R_t is the total SPR response, which is directly proportional to [A•B] + [A•B*].

Supplementary Material

Refer to Web version on PubMed Central for supplementary material.

Acknowledgments

References

Andersen C, Koronakis E, Bokma E, Eswaran J, Humphreys D, Hughes C, Koronakis V. Transition to the open state of the TolC periplasmic tunnel entrance. Proc Natl Acad Sci U S A. 2002; 99:11103–11108. [PubMed: 12163644]

Bavro VN, Pietras Z, Furnham N, Perez-Cano L, Fernandez-Recio J, Pei XY, Misra R, Luisi B. Assembly and channel opening in a bacterial drug efflux machine. Mol Cell. 2008; 30:114–121. [PubMed: 18406332]

Fernandez-Recio J, Walas F, Federici L, Venkatesh Pratap J, Bavro VN, Miguel RN, Mizuguchi K, Luisi B. A model of a transmembrane drug-efflux pump from Gram-negative bacteria. FEBS Letters. 2004; 578:5–9. [PubMed: 15581607]

Ge Q, Yamada Y, Zgurskaya H. The C-terminal domain of AcrA is essential for the assembly and function of the multidrug efflux pump AcrAB-TolC. J Bacteriol. 2009; 191:4365–4371. [PubMed: 19411330]

Husain F, Humbard M, Misra R. Interaction between the TolC and AcrA proteins of a multidrug efflux system of Escherichia coli. J Bacteriol. 2004; 186:8533–8536. [PubMed: 15576805]

Ip H, Stratton K, Zgurskaya H, Liu J. pH-induced conformational changes of AcrA, the membrane fusion protein of Escherichia coli multidrug efflux system. J Biol Chem. 2003; 278:50474–50482. [PubMed: 14523004]

Koronakis V, Eswaran J, Hughes C. Structure and function of TolC: the bacterial exit duct for proteins and drugs. Annu Rev Biochem. 2004; 73:467–489. [PubMed: 15189150]

Koronakis V, Sharff A, Koronakis E, Luisi B, Hughes C. Crystal structure of the bacterial membrane protein TolC central to multidrug efflux and protein export. Nature. 2000; 405:914–919. [PubMed: 10879525]

Levy SB, Marshall B. Antibacterial resistance worldwide: causes, challenges and responses. Nat Med. 2004; 10:S122–129. [PubMed: 15577930]

Livermore DM. The need for new antibiotics. Clin Microbiol Infect. 2004; 10(Suppl 4):1–9. [PubMed: 15522034]

Lobedanz S, Bokma E, Symmons MF, Koronakis E, Hughes C, Koronakis V. A periplasmic coiled-coil interface underlying TolC recruitment and the assembly of bacterial drug efflux pumps. Proc Natl Acad Sci U S A. 2007; 104:4612–4617. [PubMed: 17360572]

Lomovskaya O, Warren MS, Lee A, Galazzo J, Fronko R, Lee M, Blais J, Cho D, Chamberland S, Renau T, et al. Identification and characterization of inhibitors of multidrug resistance efflux pumps in Pseudomonas aeruginosa: novel agents for combination therapy. Antimicrob Agents Chemother. 2001; 45:105–116. [PubMed: 11120952]

Mikolosko J, Bobyk K, Zgurskaya HI, Ghosh P. Conformational Flexibility in the Multidrug Efflux System Protein AcrA. Structure. 2006; 14:577–587. [PubMed: 16531241]

Misra R, Bavro VN. Assembly and transport mechanism of tripartite drug efflux systems. Biochim Biophys Acta. 2009; 1794:817–825. [PubMed: 19289182]

Murakami S, Nakashima R, Yamashita E, Yamaguchi A. Crystal structure of bacterial multidrug efflux transporter AcrB. Nature. 2002; 419:587–593. [PubMed: 12374972]

Nikaido H, Takatsuka Y. Mechanisms of RND multidrug efflux pumps. Biochim Biophys Acta. 2009; 1794:769–781. [PubMed: 19026770]

Pei XY, Hinchliffe P, Symmons MF, Koronakis E, Benz R, Hughes C, Koronakis V. Structures of sequential open states in a symmetrical opening transition of the TolC exit duct. Proc Natl Acad Sci U S A. 108:2112–2117. [PubMed: 21245342]

Petrushenko ZM, Lai CH, Rybenkov VV. Antagonistic interactions of kleisins and DNA with bacterial Condensin MukB. J Biol Chem. 2006; 281:34208–34217. [PubMed: 16982609]

Piddock LJ. Multidrug-resistance efflux pumps - not just for resistance. Nat Rev Microbiol. 2006; 4:629–636. [PubMed: 16845433]

Pos KM. Drug transport mechanism of the AcrB efflux pump. Biochim Biophys Acta. 2009; 1794:782–793. [PubMed: 19166984]

Seeger MA, Schiefner A, Eicher T, Verrey F, Diederichs K, Pos KM. Structural asymmetry of AcrB trimer suggests a peristaltic pump mechanism. Science. 2006; 313:1295–1298. [PubMed: 16946072]

Sennhauser G, Amstutz P, Briand C, Storchenegger O, Grutter MG. Drug export pathway of multidrug exporter AcrB revealed by DARPin inhibitors. PLoS Biol. 2007; 5:e7. [PubMed: 17194213]

Stroebel D, Sendra V, Cannella D, Helbig K, Nies DH, Coves J. Oligomeric behavior of the RND transporters CusA and AcrB in micellar solution of detergent. Biochim Biophys Acta. 2007; 1768:1567–1573. [PubMed: 17467658]

Symmons MF, Bokma E, Koronakis E, Hughes C, Koronakis V. The assembled structure of a complete tripartite bacterial multidrug efflux pump. Proc Natl Acad Sci U S A. 2009; 106:7173–7178. [PubMed: 19342493]

Talbot GH, Bradley J, Edwards JE Jr, Gilbert D, Scheld M, Bartlett JG. Bad bugs need drugs: an update on the development pipeline from the Antimicrobial Availability Task Force of the Infectious Diseases Society of America. Clin Infect Dis. 2006; 42:657–668. [PubMed: 16447111]

Tamura N, Murakami S, Oyama Y, Ishiguro M, Yamaguchi A. Direct Interaction of Multidrug Efflux Transporter AcrB and Outer Membrane Channel TolC Detected via Site-Directed Disulfide Cross-Linking. Biochemistry. 2005; 44:11115–11121. [PubMed: 16101295]

Tikhonova EB, Dastidar V, Rybenkov VV, Zgurskaya HI. Kinetic control of TolC recruitment by multidrug efflux complexes. Proc Natl Acad Sci U S A. 2009; 106:16416–16421. [PubMed: 19805313]

Tikhonova EB, Zgurskaya HI. AcrA, AcrB, and TolC of Escherichia coli Form a Stable Intermembrane Multidrug Efflux Complex. J Biol Chem. 2004; 279:32116–32124. [PubMed: 15155734]

Touze T, Eswaran J, Bokma E, Koronakis E, Hughes C, Koronakis V. Interactions underlying assembly of the Escherichia coli AcrAB-TolC multidrug efflux system. Mol Microbiol. 2004; 53:697–706. [PubMed: 15228545]

Weeks JW, Celaya-Kolb T, Pecora S, Misra R. AcrA suppressor alterations reverse the drug hypersensitivity phenotype of a TolC mutant by inducing TolC aperture opening. Mol Microbiol. 2010; 75:1468–1483. [PubMed: 20132445]

Zgurskaya HI. Multicomponent drug efflux complexes: architecture and mechanism of assembly. Future Microbiol. 2009; 4:919–932. [PubMed: 19722844]

Zgurskaya HI, Nikaido H. AcrA is a highly asymmetric protein capable of spanning the periplasm. J Mol Biol. 1999a; 285:409–420. [PubMed: 9878415]

Zgurskaya HI, Nikaido H. Bypassing the periplasm: reconstitution of the AcrAB multidrug efflux pump of Escherichia coli. Proceedings of the National Academy of Sciences of the United States of America. 1999b; 96:7190–7195. [PubMed: 10377390]

Zgurskaya HI, Nikaido H. Multidrug resistance mechanisms: drug efflux across two membranes. Molecular Microbiology. 2000; 37:219–225. [PubMed: 10931319]

Zgurskaya HI, Yamada Y, Tikhonova EB, Ge Q, Krishnamoorthy G. Structural and functional diversity of bacterial membrane fusion proteins. Biochim Biophys Acta. 2009; 1794:794–807. [PubMed: 19041958]
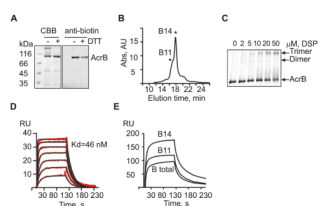
Figure 1.
Immobilization of AcrB. **(A)** Purification and biotinylation of AcrB^{S1043C}. Purified AcrB^{S1043C} (0.5 µg) and its biotinylated derivative Cys1043^{bio} were mixed with the SDS-sample buffer plus/minus 10 mM DTT and separated by 10% SDS-PAGE. Protein was either stained with Coomassie Brilliant Blue (CBB) or transferred onto PVDF membrane and incubated with streptavidin alkaline phosphatase (anti-biotin). Cys1043^{bio}–anti-biotin complex was visualized with nitro-blue tetrazolium chloride (NBT) and 5-bromo-4-chloro-3′-indolyphosphate p-toluidine (BCIP) salt substrates. **(B)** Fractionation of Cys1043^{bio} by size exclusion chromatography. Cys1043^{bio} was injected onto YM-Pack Diol-300 column at 0.5 ml/min in 20 mM Tris-HCl (pH 7.5), 150 mM NaCl, 0.03% DDM (Tris buffer). Eluted fractions (0.25 ml) were collected, of which B11 and B14 fractions were used in SPR assays. **(C)** Anti-biotin Western analysis of Cys1043^{bio} (2.3 µM) treated with indicated concentrations of the amine-reactive cross-linker dithiobis[succinimidyl propionate (DSP) in buffer containing 20 mM Hepes-KOH (7.7), 150 mM NaCl and 0.03% DDM. The reactions were carried out for 30 min at 37°C. Monomeric AcrB and its cross-linked dimers and trimers are indicated. **(D)** Kinetic analysis of DARPin binding to AcrB. Two-fold serial dilutions of DARPin (12.5–800 nM) in Tris buffer were injected over Cys1043^{bio} (AcrB thereafter) immobilized at density 2040 RU (red lines). Data were fit globally to a 1:1 Langmuir model (black), giving $k_1=1.03\times10^6$ M^{-1}s^{-1}, $k_{-1}=0.047$ s^{-1}, leading to $K_D=46$ nM. **(D)** DARPin interaction with AcrB fractions. The unfractionated Cys1043^{bio} (B total) and its B11 and B14 fractions were immobilized at densities 2384 RU, 2348 RU and 2414 RU, respectively. DARPin (100 nM) was injected at 50 µl/min for 2 min in running buffer containing 20 mM MES-KOH (pH 6.0), 150 mM NaCl, 0.03% DDM (MES buffer). See also Table 1S.
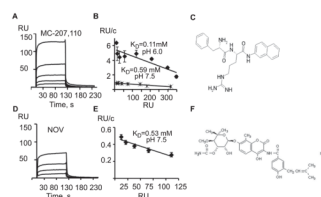
Figure 2.
Binding of inhibitors and substrates to immobilized AcrB. (**A**) Sensorgrams of twofold
dilutions 12.5–200 μM of MC-207,110 injected over AcrB surface (2040 RU) in Tris (pH
7.5) buffer. (**B**) Scatchard plots of equilibrium binding responses of MC-207,110 at pH 7.5
and pH 6.0. (**C**) Chemical structure of MC-207,110. (**D**) Sensorgrams of two-fold dilutions
25–200 μM of novobiocin (NOV) injected over AcrB surface (2040 RU) in Tris (pH 7.5)
buffer. (**E**) Scatchard plot of equilibrium binding responses of novobiocin at pH 7.5. (**F**)
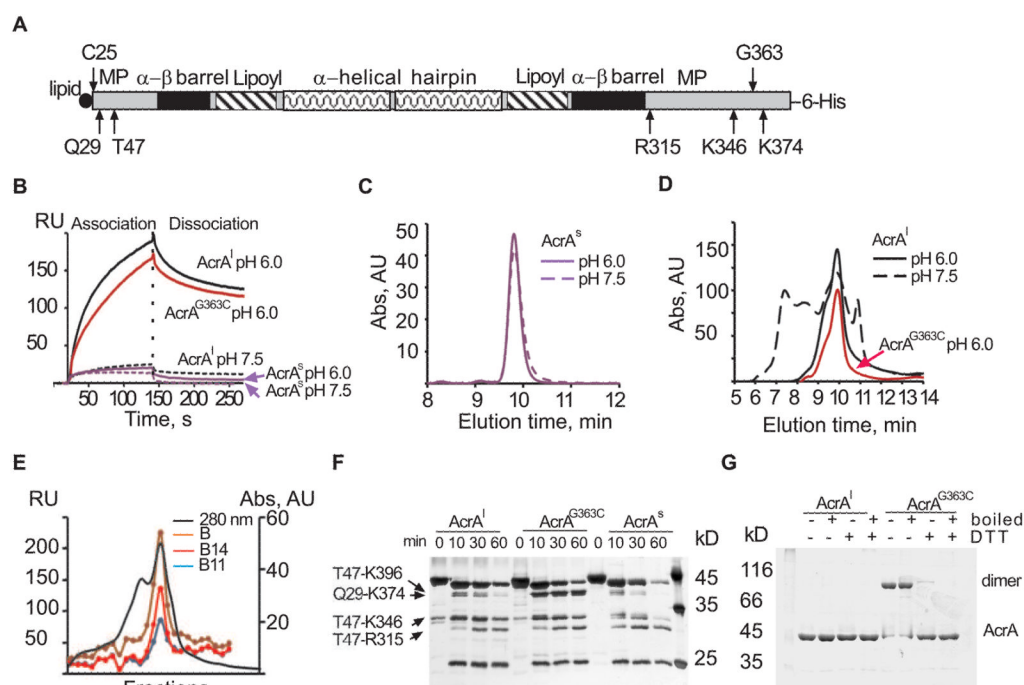Chemical structure of novobiocin.

Figure 3.
AcrA lipidation promotes oligomerization and high affinity binding to AcrB. **(A)** Graphical representation of AcrA structure with four domains and trypsin accessible sites (Ge et al., 2009) indicated. C25, the site of lipid modification, and G363 important for AcrA function are also shown. **(B)** Sensorgrams of AcrA and its derivatives. $AcrA^l$ (1 μM, black), $AcrA^{G363C}$ (1 μM, red) and $AcrA^s$ (4 μM, violet) were injected over AcrB (2040 RU) in MES pH 6.0 (solid lines) and Tris pH 7.5 buffers (dashed lines). **(C)** Size exclusion chromatography of $AcrA^s$ in MES buffer (solid line) and Tris buffer (dashed line). **(D)** Size exclusion chromatography of $AcrA^l$ in MES pH 6.0 (solid black line) and Tris pH 7.5 (dashed black line) buffers and $AcrA^{G363C}$ in MES pH 6.0 (red line). **(E)** $AcrA^l$ fractions (0.25 ml) eluted from YM-Pack Diol-300 column (280 nm, solid line) in MES buffer at 1.0 ml/min were injected over immobilized unfractionated AcrB (B) and its B11 and B14 fractions (see Figure 1 for details). Normalized equilibrium binding responses of $AcrA^l$ fractions on each AcrB surface are plotted against fraction number. **(F)** Trypsin digestion patterns of AcrA variants. Proteins (2 μM) were digested with trypsin (0.1 μM) in MES buffer at 37°C. Aliquots were taken at indicated times, mixed with SDS-sample buffer and boiled. Digestion products were resolved on 12% SDS-PAGE and silver stained. **(G)** 10% SDS-PAGE analysis of $AcrA^l$ and $AcrA^{G363C}$ under reducing and non-reducing conditions.
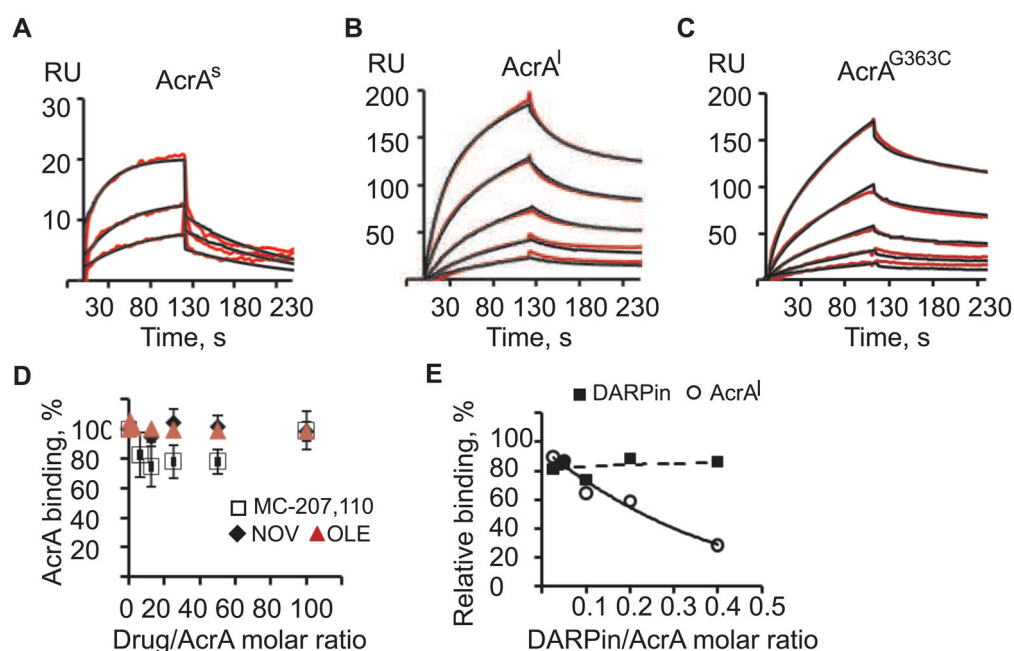
Figure 4.
Kinetic analysis of AcrA-AcrB interactions. Two-fold serial dilutions of 1.0–4.0 μM AcrA[s] **(A)**, 0.0625–1.0 μM AcrA[l] **(B)** and 0.0625–1.0 μM AcrA[G363C] **(C)** in MES buffer were injected onto AcrB (2040 RU). Sensorgrams (red lines) are fit globally using the TS model (black lines). **(D)** AcrA[l] (1.0 μM) in Tris buffer was pre-mixed with increasing concentrations of MC-207,110 (open square), NOV (black diamond) or in MES buffer with oleandomycin (red triangle), incubated at room temperature and injected over AcrB. The normalized sensorgram of AcrA[l] (1.0 μM) alone was subtracted from the sensorgrams of AcrA[l] plus inhibitor mixtures. AcrA[l] bound in the presence of drug at equilibrium (6 s before dissociation) was expressed as a percent of the AcrA[l] bound drug-free and plotted a function of a molar drug/AcrA ratio. Averages of three independent experiments and standard deviations are shown. **(E)** AcrA[l] (1.0 μM) or DARPin (0.05 μM) in MES buffer were mixed with increasing concentrations of DARPin or AcrA[l] respectively, and injected onto AcrB surface (3222 RU). Data were normalized as described in **(D).** Percents of bound DARPin (squares) and AcrA[l] (circles) in the corresponding mixtures at equilibrium are plotted as functions of DARPin/AcrA molar ratios in mixtures.
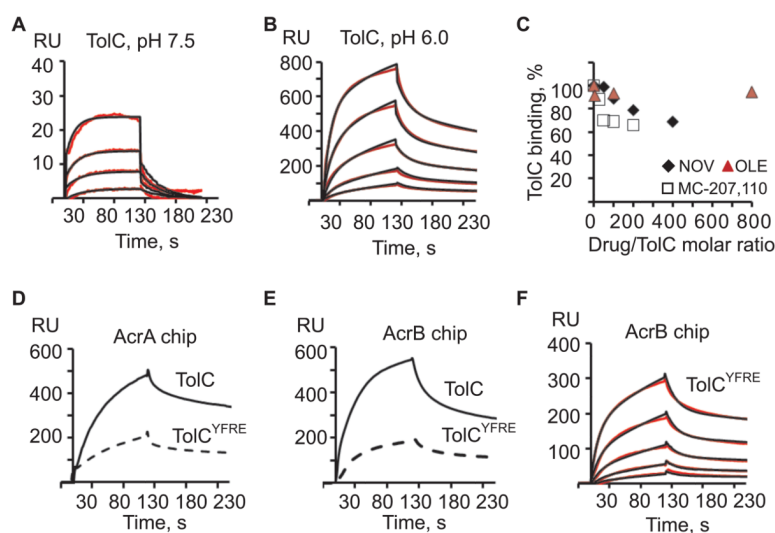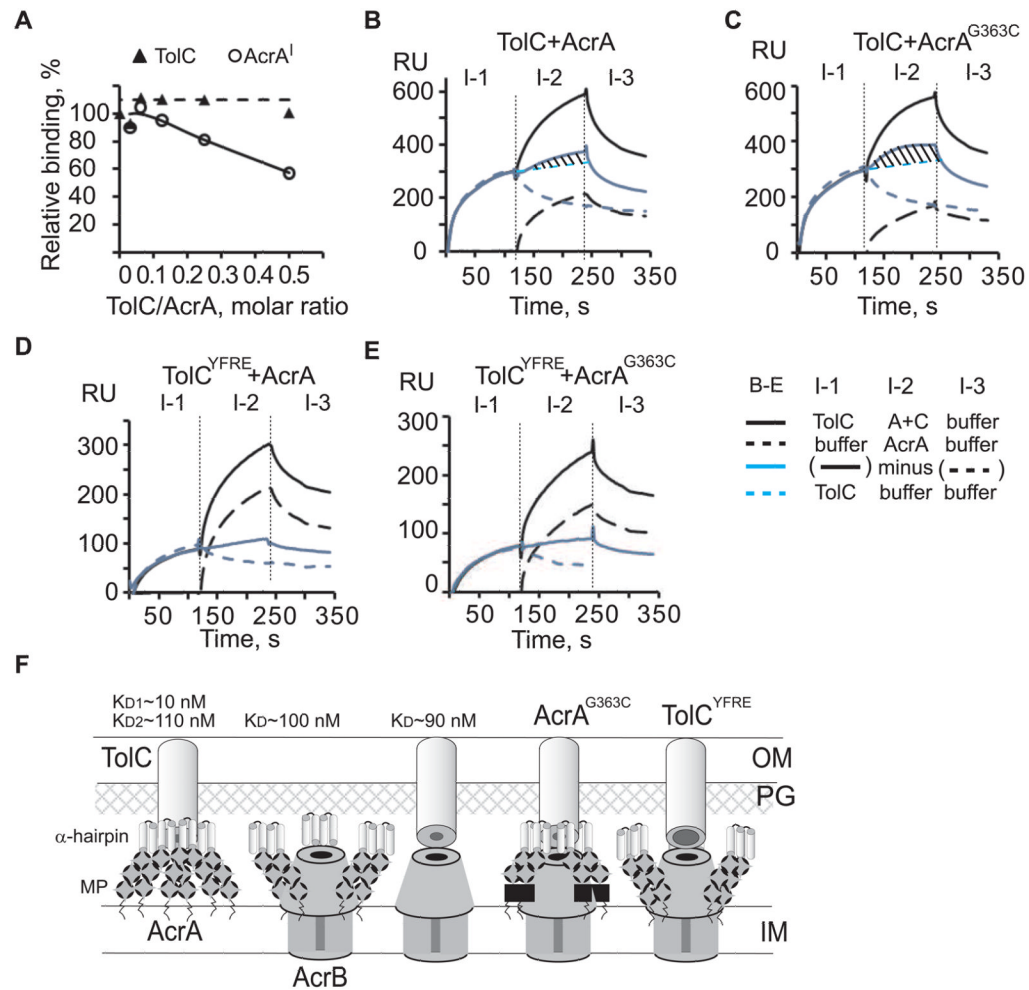
Figure 5.
Kinetic analysis of TolC-AcrB interactions. **(A)** Two-fold serial dilutions of TolC (0.03125–0.5 μM) in Tris buffer were injected onto AcrB (2040 RU). Sensorgrams (red lines) are fit globally using the 1:1 Langmuir binding (black lines). **(B)** The same as (A) but experiments were carried out in MES buffer. Data (red lines) were fit globally using the TS model (black lines). **(C)** 1.0 μM TolC in Tris buffer was pre-mixed with increasing concentrations of MC-207,110 (open squares) and NOV (black diamond), whereas 0.125 μM TolC in MES buffer was pre-mixed with oleandomycin (red triangle), incubated at room temperature and injected over AcrB. Equilibrium binding responses of TolC in the presence of a drug were expressed as percents of TolC bound in the absence of drugs and plotted as functions of a molar drug/TolC ratio. **(D)** TolC and its open TolC^{YFRE} variant (0.25 μM each) in MES buffer were injected over AcrA^{G362C} (2081 RU) surface**. (E)** The same proteins as in **(D)** injected over AcrB (2040 RU) surface. **(F)** Two-fold serial dilutions of TolC^{YFRE} (0.03125–0.5 μM) in MES buffer were injected over AcrB (2040 RU). Sensorgrams (red lines) are fit globally using the TS model (black lines).

Figure 6.
Reconstitution of AcrAB-TolC. **(A)** TolC vs. AcrA competition experiment. AcrA[l] (0.5 μM) and TolC (0.03 μM) in MES buffer were mixed with increasing concentrations of a corresponding competing analyte, incubated at room temperature and injected over AcrB (2040 RU). The equilibrium binding responses of AcrA (circles) and TolC (triangles) were expressed as percents of the bound AcrA or TolC injected alone and plotted as functions of TolC:AcrA molar ratios. To reconstitute tri-partite complexes, TolC **(B, C)** or TolC[YFRE] **(D, E)** in concentration 0.125 μM were injected alone onto AcrB (2040 RU) (I-1). Then the same concentrations of TolC variants were premixed with either AcrA[l] or AcrA[G363C] at AcrA:TolC molar ratio 8:1 and injected onto AcrB (I-2) without dissociation of the pre-assembled TolC-AcrB complexes (black solid lines). Dissociation was triggered by injecting buffer solution (I-3). The difference between normalized co-injection sensorgrams and normalized AcrA/AcrA[G363C] sensorgrams are shown by blue solid lines with the assembled tri-partite complexes indicated by shaded areas. Single analyte injections of TolC/TolC[YFRE] and AcrA/AcrA[G363C] are shown by dashed blue and black lines, respectively. **(F)** The proposed model AcrAB-TolC assembly. Bipartite AcrA-TolC, AcrA-AcrB and TolC-AcrB complexes are assembled with the same nanomolar affinities. The assembly of the tri-partite complex however requires a conformational change in the MP domain of AcrA (black squares). The opening of TolC channel decreases affinities to both AcrA and AcrB, and leads to disassembly of the complex and TolC closing. OM, outer membrane; PG, peptidoglycan; IM, inner membrane; MP, membrane proximal domain.

Table 1

Kinetic parameters of AcrB-AcrA and AcrB-TolC interactions

Analyte, µM	pH	k_1, M^{-1} s^{-1}	k_{-1}, s^{-1}	k_2, M^{-1} s^{-1}	k_{-2}, s^{-1}	K_D, µM
AcrA^s, 0.5–4.00[a]	7.5	$(1.33\pm0.22)\times10^4$	$(3.85\pm0.26)\times10^{-2}$	-	-	2.89
AcrA^s, 1.0–4.00[a]	6.0	$(6.9\pm0.09)\times10^3$	$(8.09\pm0.31)\times10^{-3}$	-	-	1.17
AcrA^l, 0.5–8.00 [a]	7.5	$(4.73\pm0.04)\times10^3$	$(2.91\pm0.06)\times10^{-3}$	-	-	0.67
AcrA^l, 0.06–1.00 [b]	6.0	$\mathbf{(2.39\pm0.06)\times10^4}$	$\mathbf{(2.1\pm0.14)\times10^{-2}}$	$\mathbf{(1.21\pm0.08)\times10^{-2}}$	$\mathbf{(1.11\pm0.26)\times10^{-3}}$	**0.09**
AcrA^{G36C}, 0.06–2.00 [b]	6.0	$\mathbf{(1.35\pm0.09)\times10^4}$	$\mathbf{(3.76\pm0.6)\times10^{-2}}$	$\mathbf{(2.9\pm0.2)\times10^{-2}}$	$\mathbf{(2.42\pm0.18)\times10^{-3}}$	**0.23**
TolC, 0.125–1.0 [a]	7.5	$(4.1\pm0.27)\times10^4$	$(3.15\pm0.09)\times10^{-2}$	-	-	0.77
TolC, 0.03–0.5 [b]	6.0	$\mathbf{(8.94\pm0.19)\times10^4}$	$\mathbf{(4.17\pm0.16)\times10^{-2}}$	$\mathbf{(1.27\pm0.04)\times10^{-2}}$	$\mathbf{(2.41\pm0.14)\times10^{-3}}$	**0.09**
TolC^{YFRE}, 0.03–0.5 [b]	6.0	$\mathbf{(5.46\pm0.03)\times10^4}$	$\mathbf{(4.8\pm0.004)\times10^{-3}}$	$\mathbf{(1.06\pm0.002)\times10^{-2}}$	$\mathbf{(1.16\pm0.002)\times10^{-3}}$	**0.10**

[a] Data were fit globally using the 1:1 Langmuir binding model.

[b] Data were fit globally using the TS model. k_{-1}, k_{-2}, k_1 and k_2 are microscopic rate constants. Equilibrium dissociation constants (K_D) were calculated from the ratio of the dissociation and association rate constants. Numbers shown in bold are for the data sets collected on the same AcrB surface (2040 RU) and on the same day.